Utilization of group 10 2D TMD-$PdSe_2$ as a nonlinear optical material for obtaining switchable laser pulse generation modes

Ping Kwong Cheng[1,2,3], Chun Yin Tang[1,2,3], Safayet Ahmed[1,2], Junpeng Qiao[1,2], Long-Hui Zeng[1,2] and Yuen Hong Tsang[1,2]

[1]Shenzhen Research Institute, The Hong Kong Polytechnic University, 518057 Shenzhen, Guangdong, People's Republic of China.

[2]Department of Applied Physics and Materials Research Center, The Hong Kong Polytechnic University, Hung Hom, Kowloon, Hong Kong, China.

[3]Ping Kwong Cheng and Chun Yin Tang contributed equally to this manuscript

E-mail: Yuen.Tsang@polyu.edu.hk

Abstract

In-plane anisotropic two-dimensional (2D) materials have gained considerable interest in the field of research, due to having the potential of being used in different device applications. Recently, among these 2D materials, group 10 transition metal dichalcogenides (TMDs) pentagonal Palladium diselenide ($PdSe_2$) is utilized in various sections of researches like nanoelectronics, thermoelectric, spintronics, optoelectronics, and ultrafast photonics, owing to its high air stability and broad absorption spectrum properties. In this paper, it is demonstrated that by utilizing this novel 2D layered $PdSe_2$ material as a saturable absorber (SA) in an Erbium-doped fiber laser (EDFL) system, it is possible to obtain switchable laser pulse generation modes. At first, the Q-switching operation mode is attained at a threshold pump power of 56.8 mW at 1564 nm, where the modulation range of pulse duration and repetition rate is 18.5 μs to 2.0 μs and 16.4 kHz to 57.0 kHz, respectively. Afterward, the laser pulse generation mode is switched to the mode-locked state at a pump power of 63.1 mW (threshold value) by changing the polarization condition inside the laser cavity, and this phenomenon persists until the maximum pump power of 230.4 mW. For this mode-locking operation, the achieved pulse duration is 766 fs, corresponding to the central wavelength and 3-dB bandwidth of 1566 nm and 4.16 nm, respectively. Finally, it is illustrated that $PdSe_2$ exhibits a modulation depth of 7.01%, which substantiates the high nonlinearity of the material.

To the best of the authors' knowledge, this is the first time of switchable modes for laser pulse generation are achieved by using this $PdSe_2$ SA. Therefore, this work will encourage the research community to carry out further studies with this $PdSe_2$ material in the future.

Keywords: $PdSe_2$, fiber laser, Q-switching, mode-locking

1. Introduction

In recent years, the study of short laser pulses has become a sustained and attractive topic in the field of laser due to its extensive applications, such as industrial processing [1,2], medical surgery [3,4], optical surveying [5,6], optical communication [7,8] and scientific research [9,10]. This short laser pulses having pulse duration from microsecond to femtosecond can be generated by utilizing the Q-switching or mode-locking technique. These different operation modes produce laser pulses with various features. Generally, Q-switching laser produces laser pulses with high energy having a pulse duration in the micron to nano second range. Mainstream applications of Q-switched lasers include laser processing, pulsed holography, metal cutting, 3D printing, distance measurement, and skin photo-rejuvenation [11-13]. Meanwhile, mode-locking lasers produce high peak power laser pulses with a much shorter pulse duration (pico to femto second region). This type of laser has many applications in nuclear fusion, terahertz radiation generation, 3D optical data storage, micro/nano machining, eye surgery, and two-photon microscopies [14-17]. Therefore, it can be determined that these two laser pulse generation modes can individually provide a significant range of advantages in industrial applications and scientific research. And it will be vital to study the possibility of achieving both operational modes within a single laser system because such a laser system can serve as a very flexible and versatile laser tool with a vast range of tunable pulse duration, which can cover a wide range of applications [18-20].

For attaining active Q-switching and mode-locking operations, an electro-optic/acousto-optic modulator (EOM/AOM) is generally used [21-23]. However, due to significant drawbacks such as slow response time, complicated synchronization process, high cost, and bulk size, these devices are limited in flexibility and applicability. On the other hand, using the nonlinear saturable absorption property of some optical materials, it is possible to generate short to ultra-short laser pulses via passive Q-switching and mode-locking operations within the laser cavity. This is an attractive technique due to having the merits of fast recovery time (shorter pulse

duration), cost-effectiveness, compactness, and self-starting mechanism [24-28]. Recently, two-dimensional (2D) layered materials have drawn enormous attention as saturable absorber on the pulsed laser generation research because of their superior nonlinear optical (NLO) response, low fabrication cost, tunable bandgap, high modulation depth, and admirable saturable absorption property [29-31]. Within the 2D materials family, the transition metal dichalcogenides (TMDs; MX_2, where M is the transition metal element and X is the chalcogenide element S, Se, and Te, respectively), are one of the most promising and prominent groups of novel materials for applying as a saturable absorber material, owing to their excellent electrical mobility [32-34] and strong NLO response [35,36].

In the past two years, the study of the 2D TMDs as SA have extended to the group 10 elements, particularly platinum (Pt) and Palladium (Pd) based TMDs (PtS_2, $PtSe_2$, $PtTe_2$, and PdS_2), due to their outstanding material properties, including excellent air stability in the ambient environment [37-39] and high carrier mobility which is comparable to graphene and black phosphorus (BP) [40-42]. However, most of these studies, based on the group 10 TMDs SAs, have exhibited generation of laser pulses through Q-switching or Mode locking technique only [37,38,43-46]. And there are only a few works that have demonstrated the production of Q-switched and mode-locked pulses altogether. For instance, Zhang et al. have shown that by using D-shaped fiber-based $PtSe_2$ SA in the Er-doped fiber cavity, it possible to obtain Q-switching and mode-locking operations by adjusting the polarization [47]. Moreover, in our previous study, we have illustrated that by using two different types of PdS_2 SAs, such as PdS_2-polyvinyl alcohol (PVA) based SA and PdS_2- side polished fiber (SPF) based SA, it is possible to obtain Q-switching and mode-locking operation, respectively [48].

Recently, a new Pd based TMD, palladium deselenide ($PdSe_2$) is getting such attention due to its functional properties. $PdSe_2$ is structured as an intriguing pentagonal morphology (Figure 1), which is different from the general hexagonal structure of TMDs. Sun et al. have shown that the indirect bandgap of monolayer and bulk $PdSe_2$ are about 1.43 eV and 0.03 eV, respectively [49]. Meanwhile, the broad absorption spectrum of PdSe2 is reported (monolayer and bilayer PdSe2 cover from the visible to ultraviolet regions), in which the applications of well-functional solar cell and photovoltaic device are demonstrated [50,51]. Besides, $PdSe_2$ has been further developed into heterojunction, which is proposed as a high-performance photodetector and imaging sensor ranging from deep ultraviolet to mid-infrared [52-54]. These

demonstrations imply that a wide operational wavelength range can be achieved by using $PdSe_2$. Moreover, $PdSe_2$ also provides a high electron field-effect mobility of about 216 $cm^2V^{-1}s^{-1}$ (comparable to $PtSe_2$, 210 $cm^2V^{-1}s^{-1}$ [40]), which is favorable to transistor applications [55,56], and indicate high performance when it is being used in optoelectronic devices and other applications. Recently, water splitting operation [57] and photodetector [58] are achieved by using $PdSe_2$, which confirms the high stability of the material. Moreover, Zhang et al. and Xu et al. demonstrated the generation of mode-locked and dissipative soliton pulses, respectively, by utilizing $PdSe_2$ as SA, which corroborates the high nonlinearity of the material [59,60].

In this study, by utilizing $PdSe_2$ as SA in an erbium-doped fiber (EDF) ring cavity system, switchable laser pulse generation modes are obtained for the first time. Here, it is demonstrated that it is possible to switch from Q-switch to Mode-lock operation and tune the laser pulses from micron second to hundreds of femtoseconds by only adjusting the polarization inside the laser cavity. Moreover, the achieved ultrafast laser pulse duration is comparable with other group 10 TMDs-SA based mode-locking operations ($PtSe_2$ [45] and PdS_2 [48]). Therefore, this work will further contribute to the development of photonic researches based on the novel group 10 TMDs materials, and due to its switchable operation capability, it will also have an enormous impact on the industrial applications.

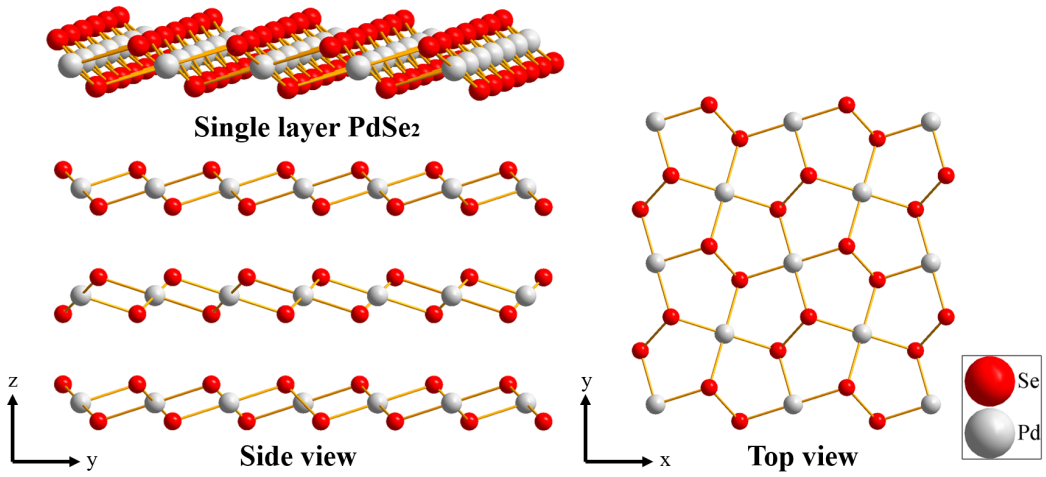

Figure 1. The atomic structure of the $PdSe_2$ layer.

2. $PdSe_2$ sample preparation and material characterization

In this work, $PdSe_2$ powder, bought from Six carbon Inc, is synthesized by the chemical vapor deposition (CVD) method. At first, the powder is ultrasonicated, after

mixing it with Isopropyl alcohol (IPA) solvent (1mg/mL of mixture ratio), at 40 kHz of frequency and 400 W of output power for about 25 hours. Then the $PdSe_2$-IPA solution is processed by using the centrifugal method at 3000 rpm of centrifugal speed for 7 minutes. This process ensured that most of the non-exfoliated materials and large substances are removed from the $PdSe_2$-IPA supernatant.

Afterward, the exfoliated $PdSe_2$ sample is coated on the quartz substrate by using a spin coating method and then dried it at 60 °C on the hot plate. Later, the samples are characterized by utilizing atomic force microscopy (AFM, Bruker Nanoscope 8) and Raman spectroscopy (WITEC_Confocal Raman system). From AFM measurement, the topological characteristics of the $PdSe_2$ sample are determined. After analyzing 280 flakes of the $PdSe_2$ as-prepared sample from AFM result, it can be illustrated that the thickness and the average lateral size of the flakes along the short axis and long axis are 31 nm, 98 nm, and 190 nm, as presented in Figure 2(a) to 2(c), respectively. Meanwhile, two $PdSe_2$ flakes are selected randomly from the topology graph, which is shown in Figure 2(d). The height profiles of two selected flakes denoted by flake A (along the long axis; green line) and flake B (along the short axis; blue line) are about 200 nm and 100 nm, respectively. The Raman spectrum, shown in Figure 2(e), is obtained after excited the $PdSe_2$ sample with a 532 nm laser. Four Raman peaks are observed, which are located around at 143.2 cm^{-1}, 204.1 cm^{-1}, 220.0 cm^{-1}, and 255.2 cm^{-1}, respectively. Based on previous results [55,61], the first three Raman peaks have matched with the modes of the movement of Se atoms and defined as A_g^1, A_g^2, and B_{1g}, while the last peak is defined as A_g^3 and assigned to the relative movements between Pd and Se atoms.

Furthermore, the sample is analyzed by utilizing field-emission transmission electron microscopy (FETEM, JEOL Model JEM-2100F). For that, the prepared $PdSe_2$-IPA supernatant is diluted with pure IPA at about 1:3 volume ratio, and then the diluted solution is dropped on the cupper grid and dried at 60 °C in the vacuum dryer for 24 hours. In Figure 3(a), the TEM image of a randomly selected flake is shown, where the lateral sizes of the chosen flake are around 103 nm in the short axis and 207 nm in the long axis, respectively. These results are well-matched with the observation of AFM measurement. Moreover, the sample is examined at a high-resolution TEM scale, which presented a few crystal lattices planes of $PdSe_2$, as shown in Figure 3(b). The lattice planes are determined as (102), (112), and (212), which are in correspondent to the d-spacing of 0.35 nm, 0.30 nm, and 0.22 nm, respectively [62]. Besides, several polymorphic rings, representing the lattice planes of $PdSe_2$, are detected from the selected area electron diffraction (SAED) pattern, as shown in Figure 3(c). These data indicated that the $PdSe_2$ sample has high crystallinity and polycrystalline characteristic. Our data are also well agreed with previously demonstrated results [62]. In Figure 3(d),

the energy-dispersive X-ray spectroscopy (EDS) spectrum of the same target sample is shown. Along with Pd and Se peaks, Cu peak is also observed in the EDS spectrum as the copper grid is used in the measurement. Besides, the atomic ratio between Pd and Se elements is determined by about 1:2 (Pd 31.3% and S 68.7%), which proves that the $PdSe_2$ sample has high purity and appropriate molecular ratio.

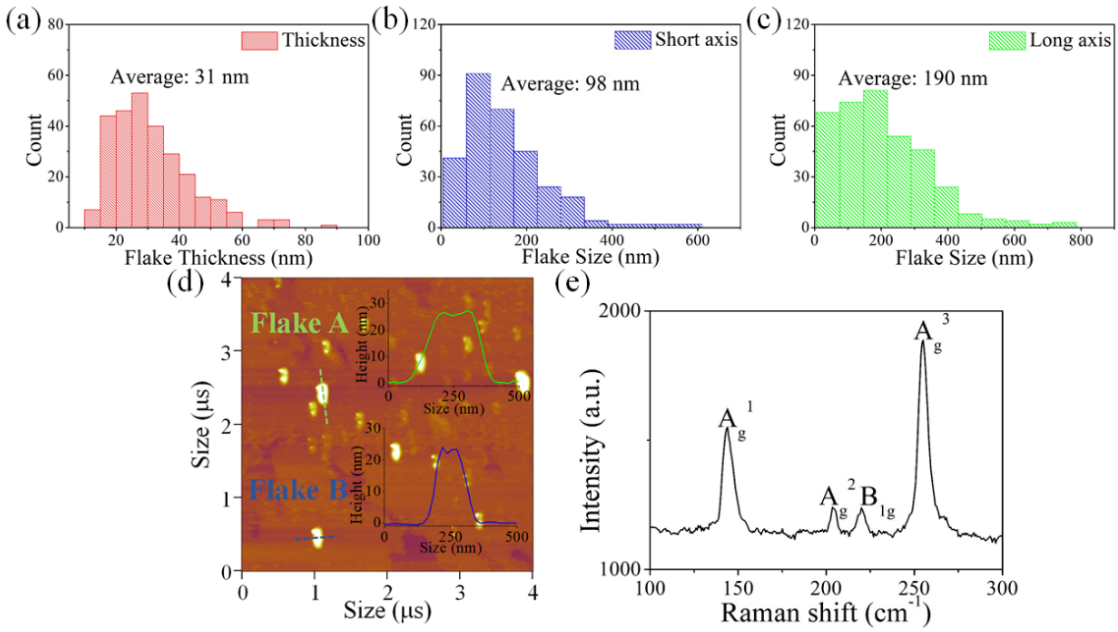

Figure 2. Statistical lateral size distribution along with (a) thickness, (b) short axis, (c) long axis of 280 $PdSe_2$ flakes; (d) An image of AFM measurement with the height profile of randomly selected Flake A and Flake B; (e) Raman spectrum of $PdSe_2$ sample.

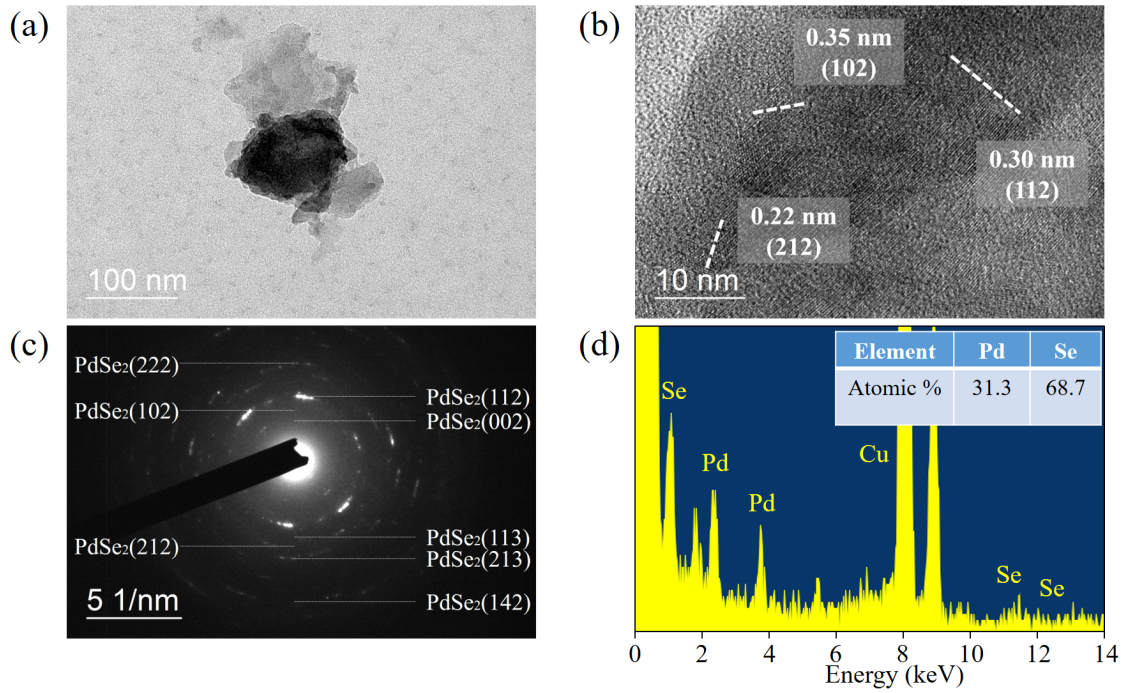

Figure 3. (a) FETEM image, (b) HRTEM image, (c) SAED pattern, and (d) EDS spectrum of randomly selected $PdSe_2$ flake.

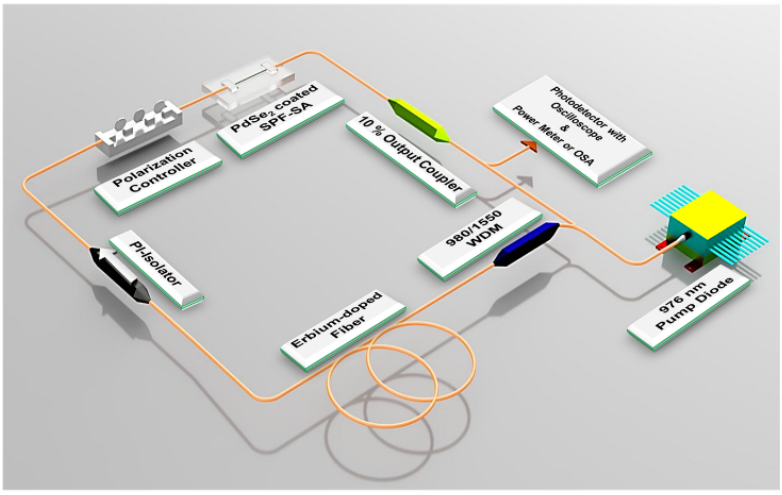

Figure 4. Er-doped fiber laser ring cavity for switchable laser pulse generation modes.

3. $PdSe_2$ based SPF-SA fabrication and fiber laser setup

A ring laser cavity system (Figure 4) is built with a total cavity length of 16.5 m, which is consisted of a 976 nm laser diode pump source, a 980/1550 nm wavelength division multiplexer (WDM), a 0.7 m Erbium-doped single-mode fiber (EDF, LIEKKI Er110-4/125), a polarization-independent isolator (PI-ISO), a 3-paddle polarization controller (PC), a 10 % output coupler (OC), 15.8 m of single-mode fiber (SMF-28)

and a $PdSe_2$ based SPF-SA. The prepared SPF has polished region length of 1 cm and thickness of the polished surface from the core is 1 μm. The dispersion of EDF and SMF-28 is recorded as about -15 ps/(nm-km) and 18 ps/(nm-km); thereby, the group velocity dispersion (GVD) is approximately 19.1 ps^2/km and -23.0 ps^2/km at 1550 nm, respectively. Moreover, the net cavity dispersion is about -0.35 ps^2. The characterizations of Q-switching and mode-locking laser operation are measured by using an optical power meter (PM20CH, Thorlabs), an oscilloscope (WaveRunner 44MXi, Teledyne LeCroy), a photodetector (DET01CFC, Thorlabs) and an optical spectrum analyzer (AQ6370B, Yokogawa).

Before dripping the $PdSe_2$-IPA solution on SPF, the output state of the laser is determined for a pump power ranging from 0 to 400 W. It is observed that without the material on SPF, no mode locking or Q-switching operations are obtained, only continuous wave (CW) laser is realized during the whole time. After that, the $PdSe_2$-SPF SA is fabricated by dripping the as-prepared $PdSe_2$-IPA solution a few times on SPF while keeping the laser cavity operating under the pump power of 400 mW. SPF provides an evanescent waveguide, which allows light to travel in the fiber core while interacting with the $PdSe_2$ sample, coated on the polished region with light-guiding self -assembling [63]. Moreover, the optical damage threshold can be enhanced due to the SPF-SA provides an evanescent field which interact with the $PdSe_2$ sample without the direct transverse light. Therefore, the sample and fiber end both can be avoid burning when the pump power is high. The laser output results obtain through utilizing this $PdSe_2$-SPF SA are presented and discussed in the following section.

4. Experimental results and discussions

4.1 Q-switched laser operation

For the laser cavity used in this study, Q-switching laser operation is observed when the pump power is increased beyond 56.8 mW, and it remains stable until the pump power is about the 354.4 mW. For this span of pump power, the average output power obtains for Q-switched laser operation is from 0.06 mW to 1.74 mW, which is presented in Figure 5(a). Moreover, by controlling the optical pump power, it is observed that the full width half maximum (FWHM) of pulse duration and the repetition rate can be modulated from 18.5 μs to 2.0 μs and 16.4 kHz to 57.0 kHz, respectively, as shown in Figure 5(b). In addition, from Figure 5(c) to 5(f), the continuous pulse train, single pulse profile, radio frequency (RF) spectrum, and wavelength spectrum can be determined for the maximum output power of 1.74 mW. A stable continuous pulse train is presented in Figure 5(c), from where the corresponding maximum single pulse energy and pulse peak power are calculated as 30.5 nJ and 15.1 mW. The RF spectrum is evaluated with

95 Hz of the resolution bandwidth, as demonstrated in Figure 5(e). And then the signal to noise ratio (SNR) is computed about 61 dB, which represents the high stability of the Q-switched operation. Moreover, the 1564 nm of central wavelength is recorded from the wave spectrum, as exhibited in Figure 5(f). From Table 1 and 2, it can be determined that the achieved pulse duration and SNR are comparable to the other group 10 TMDs SAs, as well as the modulation range of repetition rate and pulse duration are compare with other type of SAs, which indicates that $PdSe_2$ is a good SA material for Q-switching pulses generation.

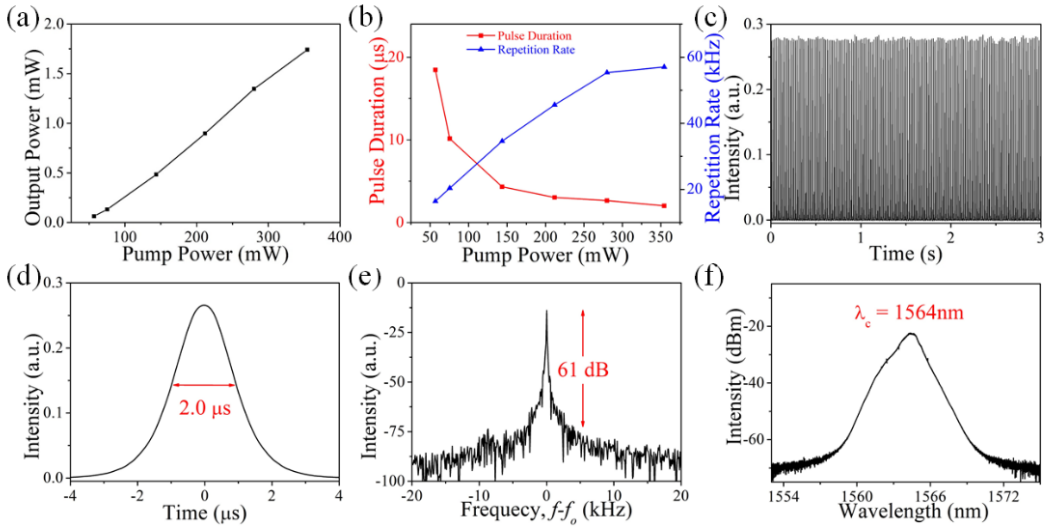

Figure 5. The optical performance of Q-switching operation: (a) average output power, (b) pulse duration and repetition rate correspondence to various optical pump power; (c) output pulse train, (d) single pulse profile, (e) radio frequency, and (f) wavelength spectrum at the maximum output power.

4.2 Mode-locked laser operation

After obtaining the Q-switched laser pulses, the operation mode of the laser cavity is switched to mode-locking by modifying the intracavity polarization state with the PC, for the optical pump power of 63.1 mW (threshold value). Afterward, by tuning the pump power up to 230.4 mW, the average output power is varied from 0.03 mW to 0.56 mW, as demonstrated in Figure 7(a). The pulse train in different time scales, autocorrelation trace, RF spectrum, and wavelength spectrum are also measured for the maximum output power state as presented in Figure 7(b) to 7(f). Regular CW envelope pulse train (Figure 7(b)) suggest that mode-locked operation is highly stable. Moreover, the recorded roundtrip cavity time of the mode-locked pulse is about 79.8 ns, as shown in Figure 7(c), which agrees with the total cavity length. Additionally, in Figure 7(d), the mode-locking pulse duration is illustrated, which is measured by utilizing an

autocorrelator (FR-103XL, Femtochrome Research. Inc.), and the result of the autocorrelation trace is fitted with the squared hyperbolic secant ($sech^2$) function. Therefore, the obtained 1.18 ps of FWHM trace represents that the exact pulse duration is about 766 fs, which is comparable with other group 10-TMDs based SA studies, as presented in Table 1. Moreover, the corresponding maximum single pulse energy and pulse peak power are calculated as 44.8 pJ and 51.5 W for the $sech^2$ pulse. Meanwhile, the measured fundamental repetition rate and SNR are about 12.5 MHz and 61 dB, respectively. As shown in Table 1, the value of SNR is comparable to other TMDs SA results (PtS_2, 43 dB [37]; $PtSe_2$, 54 dB [38]; PdS_2, 53 dB [48]), and it also indicates the high stability of the mode-locking operation. Also, the central wavelength and the 3 dB bandwidth of the wavelength spectrum are illustrated as 1566 nm and 4.16 nm, respectively, as demonstrated in Figure 7(f). Therefore, the time-bandwidth product (TBP) is calculated as about 0.390, which is higher than the value of the classical bandwidth-limited pulse of 0.315 [73]. Hence, the pulse duration can be further compressed by optimizing the laser cavity. Furthermore, the durability of $PdSe_2$ based SA is also tested, where the fluctuation of the average output power is about 5 %, and the wavelength spectrum has remained in the same shape for more than 60 minutes as shown in Figure 6.

4.3 Illustration of saturable absorption property and switching operation

The nonlinear optical performance of the functional $PdSe^2$ based SPF-SA is characterized by utilizing a balanced twin-detector system with an ultrafast laser source (pulse duration of 2 ps and repetition rate of 12.1 MHz) at a wavelength of 1560 nm as shown in Figure 8. The maximum insertion loss and polarization-dependent loss of $PdSe_2$ based SPF-SA are measured by about 6.6 dB and 4.3 dB, respectively. Moreover, the saturable absorption property of $PdSe_2$ based SPF-SA is measured and fitted by using an exponential relationship [74], which is shown in Figure 9. The saturable intensity and modulation depth of the $PdSe_2$ based SPF-SA are estimated as about 1.87 GW/cm^2 and 7.01 % (Figure 9(a)), respectively, in the transverse electric (TE) mode; and 2.41 GW/cm^2 and 2.37 % (Figure 9(b)), respectively, in the transverse magnetic (TM) mode [73]. As the polarization of TE mode is in parallel to the $PdSe_2$ coating surface, thereby the evanescent field gains the highest interaction with the sample. In contrast, the polarization of TM mode is vertical to the coating surface and therefore exhibits the lowest interaction [75]. Consequently, it can be determined that changing the polarization state is a vital criterion for adjusting the output mode of the laser cavity. Here, it is observed that the laser operation mode can be switched from the Q-switched

state to the mode-locked state and vice versa, by adjusting the polarization condition inside the laser cavity, when the pump power is between 63.1 mW to 230.4 mW. And as the operational mode is switched, the output power is also altered. From the experimental results, it can be determined that the output power of the mode-locking operation is less than the output power of the Q-switching operation under the same pump power. Therefore, it indicates that mode-locking operation is achieved when the $PdSe_2$ based SPF-SA provides a larger transmittance modulation and higher intracavity loss. In this work, the PC has functioned as a manually tunable phase retarder, which can provide optimized phase retardation and transmission loss for achieving the requirement to obtain mode-locking operation [76,77]. Hence, the mode-locking operation can be switched from Q-switching mode by adjusting the transverse mode of propagating light to be TE mode by modifying the PC position.

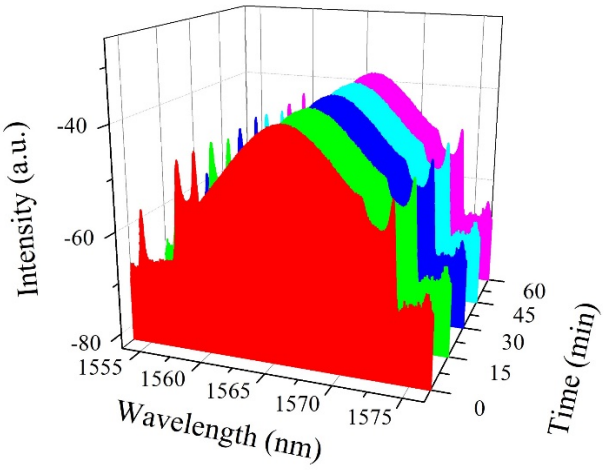

Figure 6. Spectrum stability of mode-locking operation.

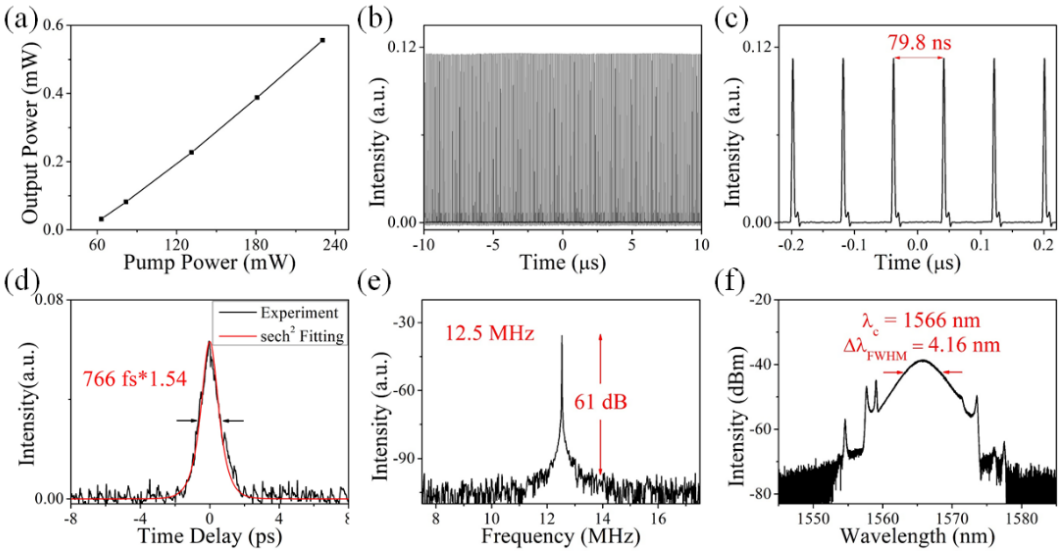

Figure 7. The optical performance of mode-locking operation: (a) average output power for various optical pump power, (b) and (c) pulse train with different time scale (d) autocorrelation trace, (e) radio frequency, and (f) wavelength spectrum at 0.56 mW output power

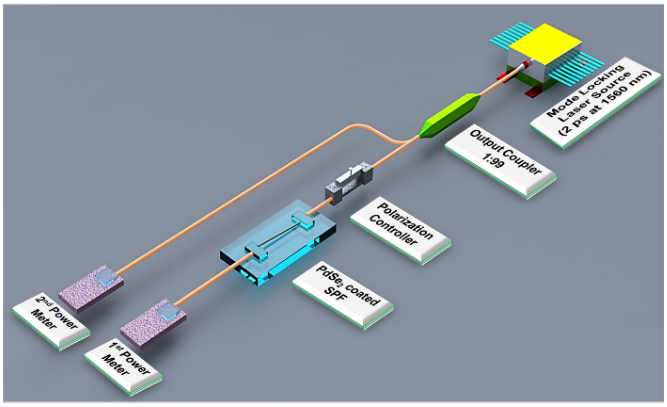

Figure 8. Balanced twin-detector system (for measuring nonlinear transmittance).

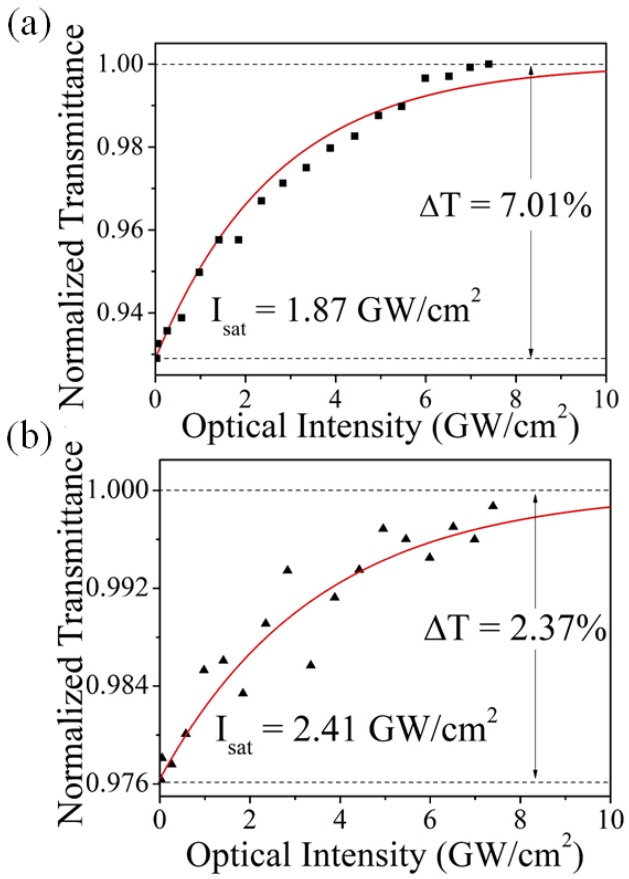

Figure 9. The nonlinear optical performance of normalized transmittance regarding various incident optical intensity at (a) maximum and (b) minimum modulation depth by TE and TM polarization condition.

Table 1. The optical performance of passive Q-switching and mode-locking operations about group 10 elements based TMDs. (TDF is thulium-doped fiber; EDF is erbium-doped fiber; YDF is ytterbium-doped fiber; SNR is signal to noise ratio)

	Material	Wavelength (Gain media)	Pulse duration (SNR)	Modulation depth	Ref.
Q-switching					
	NiS_2	1562 nm (EDF)	237 ns (/)	5.3%	[64]
	NiS_2	1916 nm (TDF)	505 ns (/)	4.3%	[64]

	PtS_2	1569 nm (EDF)	4.2 μs (/)	/	[43]
	$PtSe_2$	1560 nm (EDF)	0.9 μs (/)	4.9%	[47]
	$PtSe_2$	1563 nm (EDF)	5.9 μs (41.1 dB)	6.9%	[45]
	$PtTe_2$	1066 nm (YDF)	5.2 μs (35 dB)	/	[39]
	PdS_2	1567 nm (EDF)	4.5 μs (50 dB)	/	[48]
	$PdSe_2$	1064 nm (Nd:GdLaNbO4)	340 ns (/)	22.9%	[65]
	$PdSe_2$	1564 nm (EDF)	2.0 μs (61 dB)	2.37%	This work
Mode-locking					
	NiS_2	1064.5 nm (YDF)	11.7 ps (66 dB)	23%	[66]
	NiS_2	1560.2 nm (EDF)	524 fs (67 dB)	30.8%	[66]
	PtS_2	1572 nm (EDF)	2.06 ps (43 dB)	7%	[37]
	$PtSe_2$	1067 nm (Nd:LuVO4)	15.8 ps (/)	12.6%	[44]
	$PtSe_2$	1064 nm (Nd:YAG)	27 ps (54 dB)	1.9%	[38]
	$PtSe_2$	1560 nm (EDF)	1.02 ps (61 dB)	4.9%	[47]
	$PtSe_2$	1567 nm (EDF)	861 fs (61.1 dB)	6.9%	[45]

$PtSe_2$	1064 nm (YDF)	470 ps (53 dB)	26%	[46]
PdS_2	1565.8 nm (EDF)	803 fs (53 dB)	1.7%	[48]
$PdSe_2$	1561.8 nm (EDF)	324 fs (58 dB)	9.7%	[59]
$PdSe_2$	1067.4 nm (YDF)	768 ps (61 dB)	22.1%	[59]
$PdSe_2$	1533.6 nm (EDF)	1.19ps (55 dB)	6.2%	[60]
$PdSe_2$	1566 nm (EDF)	766 fs (61 dB)	7.01%	This work

Table 2. The optical performance of passive Q-switching EDFL operation by using various type of saturable absorbers.

Material		Modulation range		Maximum operation		Ref.
		Repetition Rate (kHz)	Pulse duration (μs)	Single pulse energy	Pulse peak power	
Organic	Alq3	15.9 – 68.0	8.5 – 6.0	139 nJ	23.2 mW	[67]
	FIrpic	39.2 – 87.4	9.5 – 3.4	123 nJ	36.2 mW	[68]
NTs	CNT	14.5 – 141	4.0 – 0.33	7.3 nJ	22.1 mW	[69]
NPs	Fe3O4	21.7 - 128	2.4 – 0.61	321 nJ	526 mW	[70]
	Ag	13.8 – 39.2	5.9 – 3.4	7.8 nJ	2.28 mW	[71]
2D layered	Graphene	10.36 – 41.8	8.4 – 2.4	28.7 nJ	10.3 mW	[72]
	BP	6.98 – 15.8	39.8 – 10.3	94.3 nJ	9.14 mW	[31]
	PdSe2	16.4 - 57.0	18.5 - 2.0	30.5 nJ	15.1 mW	This work

5. Conclusion

In summary, in this study $PdSe_2$ based SPF-SA is fabricated and utilized within an Er-doped ring laser cavity. Then it is demonstrated that the laser generation mode can be switched from passive Q-switch to mode-lock by modifying the polarization state of the laser cavity when the pump power is between 63.1 mW to 230.4 mW. Throughout the Q-switched state (centered at 1564 nm), as the pump power is increased from 56.8 mW to 354.4 mW, the average output power is changed from 0.06 mW to 1.74 mW, while the corresponding pulse duration and repetition rate are modulated from 18.5 μs to 2.0 μs and from 16.4 kHz to 57.0 kHz, respectively. Additionally, the mode-locking operation with a central wavelength of 1566 nm and 3-dB bandwidth of 4.6 nm, is achieved with the threshold pump power of 63.1 mW, and the corresponding pulse duration is measured about 766 fs with SNR of 61 dB, which is comparable with other group 10 based 2D TMDs-SA mode-locking operations. Therefore, these findings and the switchable capability between laser generation modes suggest that 2D-$PdSe_2$ can be further utilized in nonlinear optical applications and industrial investigations.

Acknowledgements

This work is financially supported by the Research Grants Council of Hong Kong, China (GRF 152093/18E). The Hong Kong Polytechnic University Shenzhen Research Institute, Shenzhen, China (Grant Code: the science and technology innovation commission of Shenzhen (JCY20180306173805740)).

References

[1]Bliedtner J, Schindler C, Seiler M, Wächter S, Friedrich M and Giesecke J 2016 Laser Tech. J 5 46–50

[2]Geng Y, Akbari M, Karimipour A, Karimi A, Soleimani A and Afrand M 2019 Infrared Phys. Technol. 103 103081

[3]Ashforth S A, Oosterbeek R N, Bodley O L, Mohr C, Aguergaray C and Simpson M C 2020 Lasers Med. Sci. 35 1263–70

[4]Landa F J O, Deán-Ben X L, de Espinosa F M and Razansky D 2016 Opt. Lett. 41 2704–7

[5]Qiu Y, Xie Y, Wang W, Liu W, Kuang L, Bai X, Hu M and Ho J 2019 2019 IEEE 4th Optoelectronics Global Conf. (https://doi.org/10.1109/OGC.2019.8925087)

[6]Bartholomew J, Lyman P C, Weimer C and Ruppert L 2017 AIAA Information Systems-AIAA Infotech@ Aerospace 0645 (https://doi.org/10.2514/6.2017-0645)
[7]McKenzie T, Dalgleish F, Vuorenkoski A, Ouyang B, Britton W, Ramos B and Shirron J 2018 OCEANS 2018 MTS/IEEE (Charleston) (https://doi.org/10.1109/OCEANS.2018.8604566)
[8]Zhan W, Hao Z, Li R, Tang Y and Wang Y 2019 Cluster Comput. 22 14451–60
[9]Gedvilas M, Mikšys J, Berzinš J, Stankevič V and Račiukaitis G 2017 Sci. Rep. 7 1–10
[10] Shih C Y, Wu C, Shugaev M V and Zhigilei L V 2017 J. Colloid Interface Sci. 489 3–17
[11] Skorczakowski M et al 2010 Laser Phys. Lett. 7 498–504
[12] Cui N et al 2020 Nanoscale 12 1061–6
[13] Yao Y et al 2019 RSC Adv. 9 14417–21
[14] Whitenett G, Stewart G, Yu H and Culshaw B 2004 J. Lightwave Technol. 22 813–9
[15] Lach E et al 1996 Proc. of European Conf. on Optical Communication IEEE
[16] Curley P F, Ferguson A I, White J G and Amos W B 1992 Opt. Quantum Electron 24 851–9
[17] Ohno T, Sato K, Fukushima S, Doi Y and Matsuoka Y 2000 J. Lightwave Technol. 18 44–9
[18] Kuizenga D J, Phillion D W, Lund T and Siegman A E 1973 Opt. Commun. 9 221–6
[19] Wu K, Zhang X, Wang J, Li X and Chen J 2015 Opt. Express 23 11453–61 8 Nanotechnology 32 (2021) 055201 P K Cheng et al
[20] Hideur A, Chartier T, Brunel M, Salhi M, Özkul C and Sanchez F 2001 Opt. Commun. 198 141–6
[21] El-Sherif A F and King T A 2003 Opt. Commun. 218 337–44
[22] Chen X, Xu H, Han W, Yi H, Yu H, Zhang H and Liu J 2015 Opt. Laser Technol. 70 128–30
[23] Delgado-Pinar M, Zalvidea D, Diez A, Pérez-Millán P and Andrés M V 2006 Opt. Express 14 1106–12
[24] Martinez A, Fuse K and Yamashita S 2011 Appl. Phys. Lett. 99 121107
[25] Tang C Y, Cheng P K, Tao L, Long H, Zeng L H, Wen Q and Tsang Y H 2017 J. Lightwave Technol. 35 4120–4
[26] Mao D, Cui X, Gan X, Li M, Zhang W, Lu H and Zhao J 2017 IEEE J. Sel. Top. Quantum Electron. 24 1–6

[27] Ibarra-Escamilla B, Durán-Sánchez M, Posada-Ramírez B, Álvarez-Tamayo R I, Alaniz-Baylón J, Bello-Jiménez M, Prieto-Cortés P and Kuzin E A 2018 IEEE Photon. Technol. Lett. 30 1768–71

[28] Prieto-Cortés P, Álvarez-Tamayo R I, García-Méndez M, Durán-Sánchez M, Barcelata-Pinzón A and Ibarra-Escamilla B 2019 Laser Phys. Lett. 16 045101

[29] Zhang H, Tang D Y, Zhao L M, Bao Q L, Loh K P, Lin B and Tjin S C 2010 Laser Phys. Lett. 7 591

[30] Lu B, Chen H, Jiang M, Chen X, Ren Z and Bai J 2013 Laser Phys. 23 045111

[31] Chen Y et al 2015 Opt. Express 23 12823–33

[32] Aji A S, Solís-Fernández P, Ji H G, Fukuda K and Ago H 2017 Adv. Funct. Mater. 27 1703448

[33] Movva H C P, Rai A, Kang S, Kim K, Fallahazad B, Taniguchi T, Watanabe K, Tutuc E and Banerjee S K 2015 ACS Nano 9 10402–10

[34] Wu W, De D, Chang S C, Wang Y, Peng H, Bao J and Pei S S 2013 Appl. Phys. Lett. 102 142106

[35] Zhang H, Lu S B, Zheng J, Du J, Wen S C, Tang D Y and Loh K P 2014 Opt. Express 22 7249–60

[36] Zhang S et al 2015 ACS Nano 9 7142–50

[37] Long H, Tang C Y, Cheng P K, Wang X Y, Qarony W and Tsang Y H 2018 J. Lightwave Technol. 37 1174–9

[38] Li Z, Li R, Pang C, Dong N, Wang J, Yu H and Chen F 2019 Opt. Express 27 8727–37

[39] Cheng P K, Tang C Y, Wang X Y, Ma S, Long H and Tsang Y H 2019 Sci. Rep. 9 1–7

[40] Zhao Y et al 2017 Adv. Mater. 29 1604230

[41] Rudenko A N, Brener S and Katsnelson M I 2016 Phys. Rev. Lett. 116 246401

[42] Bolotin K I, Sikes K J, Jiang Z, Klima M, Fudenberg G, Hone J, Kim P and Stormer H L 2008 Solid State Commun. 146 351–5

[43] Wang X, Cheng P K, Tang C Y, Long H, Yuan H, Zeng L, Ma S, Qarony W and Tsang Y H 2018 Opt. Express 26 13055–60

[44] Tao L, Huang X, He J, Lou Y, Zeng L, Li Y, Long H, Li J, Zhang L and Tsang Y H 2018 Photon. Res. 6 750–5

[45] Huang B, Du L, Yi Q, Yang L, Li J, Miao L, Zhao C and Wen S 2019 Opt. Express 27 2604–11

[46] Yuan J et al 2018 ACS Appl. Mater. Interfaces 10 21534–40

[47] Zhang K, Feng M, Ren Y, Liu F, Chen X, Yang J, Yan X Q, Song F and Tian J 2018 Photon. Res. 6 893–9
[48] Cheng P K, Tang C Y, Wang X Y, Zeng L H and Tsang Y H 2020 Photon. Res. 8 511–8
[49] Sun J, Shi H, Siegrist T and Singh D J 2015 Appl. Phys. Lett. 107 153902
[50] Kuklin A V and Agren H 2019 Phys. Rev. B 99 245114
[51] Lei W, Zhang S, Heymann G, Tang X, Wen J, Zheng X, Hu G and Ming X 2019 J. Mater. Chem. C 7 2096–105
[52] Luo L B, Wang D, Xie C, Hu J G, Zhao X Y and Liang F X 2019 Adv. Funct. Mater. 29 1900849
[53] Wu D, Jia C, Zeng L, Lin P, Dong L, Shi Z, Tian Y, Li X and Jie J 2020 J. Mater. Chem. A 8 3632–42
[54] Wu D et al 2019 ACS Nano 13 9907–17
[55] Chow W L et al 2017 Adv. Mater. 29 1602969
[56] Bartolomeo A D, Pelella A, Urban F, Grillo A, Iemmo L, Passacantando M, Liu X and Giubileo F 2020 Adv. Electron. Mater. 6 2000094
[57] Long C, Liang Y, Jin H, Huang B and Dai Y 2018 ACS Appl. Energy Mater. 2 513–20
[58] Zeng L H et al 2019 Adv. Funct. Mater. 29 1806878
[59] Zhang H, Ma P, Zhu M, Zhang W, Wang G and Fu S 2020 Nanophotonics 9 2557–67
[60] Xu N, Wang H, Zhang H, Guo L, Shang X, Jiang S and Li D 2020 Nanophotonics 9 4295–4306
[61] Zeng L H et al 2019 Adv. Sci. 6 1901134
[62] Kristin P 2014 United States 11
[63] Galeotti F, Pisco M and Cusano A 2018 Nanoscale 10 22639–3202
[64] Li S et al 2019 Opt. Express 27 19843–51
[65] Ma Y, Zhang S, Ding S, Liu X, Yu X, Peng F and Zhang Q 2020 Opt. Laser Technol. 124 105959
[66] Wang P et al 2020 Opt. Laser Technol. 132 106492
[67] Samsamnun F S, Zulkipli N F, Khudus M I, Shuhaimi A, Majid W H and Harun S W 2020 Microw. Opt. Technol. Lett. 62 1028–32
[68] Salam S, Al-Masoodi A H H, Al-Hiti A S, Al-Masoodi A H, Wang P, Wong W R and Harun S W 2019 Opt. Fiber Technol. 50 256–62
[69] Dong B, Hao J, Hu J and Liaw C Y 2010 IEEE Photon. Technol. Lett. 22 1853–5
[70] Chen Y, Yin J, Chen H, Wang J, Yan P and Ruan S 2017 IEEE Photon. J 9 1–9

[71] Ahmad H, Ruslan N E, Ali Z A, Reduan S A, Lee C S J, Shaharuddin R A, Nayan N and Ismail M A 2016 Opt. Commun. 381 85–90
[72] Wang J, Luo Z, Zhou M, Ye C, Fu H, Cai Z, Cheng H, Xu H and Qi W 2012 IEEE Photon. J. 4 1295–305
[73] Hong S et al 2018 Laser Photonics Rev. 12 1800118
[74] Lau K Y, Muhammad F D, Latif A A, Bakar M A, Yusoff Z and Mahdi M A 2017 Opt. Laser Technol. 94 221–7
[75] Lee E J et al 2015 Nat. Commun. 6 1–6
[76] Lin K H, Kang J J, Wu H H, Lee C K and Lin G R 2009 Opt. Express 17 4806–14
[77] Lee J, Koo J, Cebnath P, Song Y W and Lee J H 2013 Laser Phys. Lett. 10 035103